Two-Dimensional Highly Sensitive Wireless Displacement Sensor With Bilayer Graphene-Based Frequency Selective Surface

Jun-Jie Zhang, Bian Wu, *Senior Member, IEEE*, Yu-Tong Zhao, Lei Song, Hao-Ran Zu, Rong-Guo Song, and Da-Ping He

***Abstract*—In this paper, a two-dimensional wireless displacement sensor with high sensitivity composed of a bilayer graphene-based frequency selective surface (FSS) is proposed. The lengths of the strip-type resonators on the top and bottom layers of the FSS are different and perpendicular to each other. Based on the resonance and polarization characteristics of the FSS, two-dimensional displacement sensing can be realized. It is well validated both in simulation and experiment that the direction of the displacement can be distinguished by the variation trend of the resonant frequencies of the top and bottom layers. In experiment, the measured results of the FSS based wireless displacement sensor in the dynamic range of 5mm show high sensitivity of 280 MHz/mm in x direction and 370 MHz/mm in y direction. Moreover, the excellent mechanical and chemical stability of the multi-layer graphene also makes it suitable for harsh environments, showing good prospects in application.**

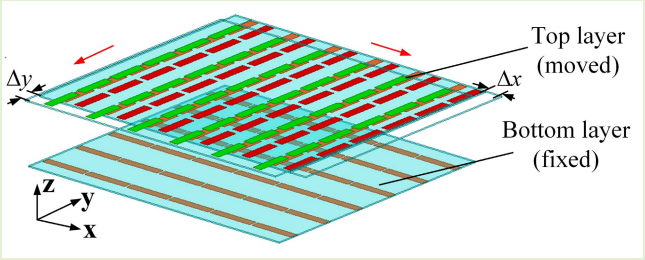

***Index Terms*—Displacement sensor, two-dimensional, high sensitivity, wireless sensor, graphene-based frequency selective surface.**

I. Introduction

With the development of microwave sensor technology, displacement sensor based on electromagnetic principle has been wildly concerned because of its easy realization, low cost and good sensing characteristics. Regardless of the alignment type or the rotation type, most microwave displacement sensors are realized by the shift of resonant frequency or the modification of magnitude at the resonant frequency. At present, more and more attention has been attracted by sensors based on coplanar waveguide (CPW) transmission line, in which CPW is combined with different resonators, such as different forms of Split-ring resonators (SRRs) [1]–[4], Electromagnetic Band Gap (EBG) structure [5], [6] and Defected Ground Structure (DGS) [7]. Except the CPW transmission line, the microstrip line loaded with resonators is also applied to displacement sensor [8]–[11].

And there are other microwave devices applied to displacement sensor, such as microstrip impedance transformer [12], resonance based [13], [14], antenna [15], [16] and radar [17], where the displacement also has a direct impact on the resonant characteristics of the sensor.

Although the microwave displacement sensors above have advantages of high sensitivity, large dynamic range as well as easier implementation, most of them need many cables to get sensing information in experiment, which is still inconvenient for operation. Therefore, it is necessary to design a non-contact and wireless sensor, and some systems with wireless communication ability can be applied to achieve wireless sensing, such as inductive coupling [18] and Radio Frequency Identification (RFID) technology [19].

It is well known that frequency selective surface (FSS) is a two-dimensional structure composed of periodic unit. It can be seen as a kind of spatial filter and has been widely used as radome [20], absorber [21], [22] and antenna [23]. And it should be noted that no coaxial cable is required to measure the electromagnetic properties, therefore it has potential for wireless sensor design. For example, because the electromagnetic characteristic of FSS is dependent on the physical dimension and dielectric properties, there has been

Manuscript received June 10, 2021; revised August 20, 2021; accepted September 24, 2021. Date of publication September 29, 2021; date of current version October 29, 2021. This work was supported in part by the National Natural Science Foundation of China (NSFC) under Grant 61771360, Grant U19A2055, Grant 62071357, and Grant 62171348; in part by the Key Industry Chain Project of Shaanxi Province under Grant 2018ZDCXL-GY-08-03-01; and in part by the Fundamental Research Funds for the Central Universities and the Innovation Fund of Xidian University. The associate editor coordinating the review of this article and approving it for publication was Prof. Tien-Kan Chung. *(Corresponding author: Bian Wu.)*

Jun-Jie Zhang, Bian Wu, Yu-Tong Zhao, Lei Song, and Hao-Ran Zu are with the National Key Laboratory of Antennas and Microwave Technology, Xidian University, Xi'an 710071, China (e-mail: bwu@mail.xidian.edu.cn).

Rong-Guo Song and Da-Ping He are with Hubei Engineering Research Center of RF-Microwave Technology and Application, Wuhan University of Technology, Wuhan 430070, China (e-mail: hedaping@whut.edu.cn).

Digital Object Identifier 10.1109/JSEN.2021.3116457

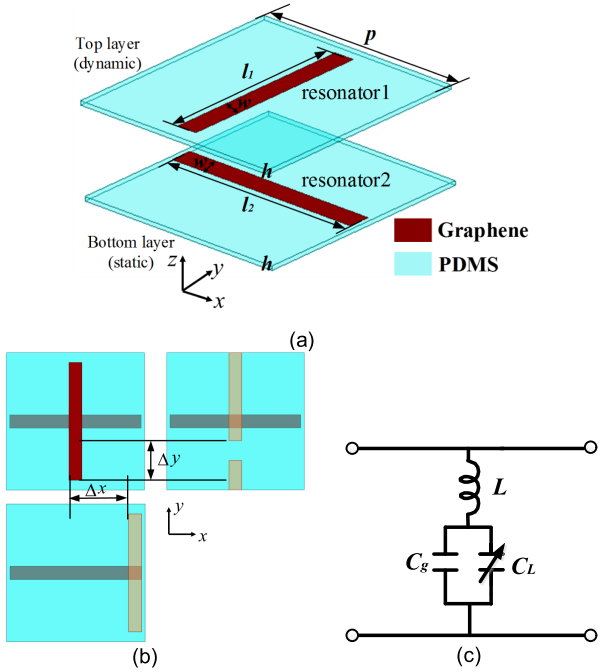

Fig. 1. The proposed bilayer FSS displacement sensor. (a) Structure of the unit cell; (b) Schematic diagram with displacement in x or y- direction; (c) Equivalent circuit of the unit cell.

some researches about FSS or metamaterial based sensors, such as the thin-film sensor [24], [25], biological sensor [26], strain sensor [27], displacement sensor [28] and other sensors [29], [30], showing advantages of wireless sensing, low cost and good performance.

Based on two-dimensional FSS, two-dimensional displacement sensor can be realized, which is more reliable and accurate than one-dimensional displacement sensing results. It can be applied to the periodic structural health monitoring (SHM) of bridges, tunnels and other buildings to detect the degree of deformation of engineering buildings during construction and operation [31].

In this paper, a multi-layer graphene based FSS with two layers is used to design a two-dimensional and highly sensitive wireless displacement sensor. Because the resonators on the top and bottom layer of the FSS are strip-type and perpendicular to each other, the double-layer FSS shows resonance and the polarization dependency characteristic, which can be applied to a two-dimensional displacement sensor design theoretically. And both the simulation and experiment successfully validate that the FSS based displacement sensor can distinguish the direction of the displacement and shows high sensitivity in each direction. Furthermore, the displacement sensor can not only be measured wirelessly, but also work in harsh environments and extend service life due to the lightweight, mechanical stability and chemical resistance of the graphene film.

II. Design and Analysis

The unit cell of the double-layer graphene-based FSS with period of p=10.5mm is shown in Fig. 1 (a), where the optimized dimensions of the unit cell are summarized in Table I.

TABLE I
DIMENSIONS OF THE BILAYER FSS

Symbol	p	l_1	l_2	w	h
Dimension(mm)	10.5	9	10	2	0.2

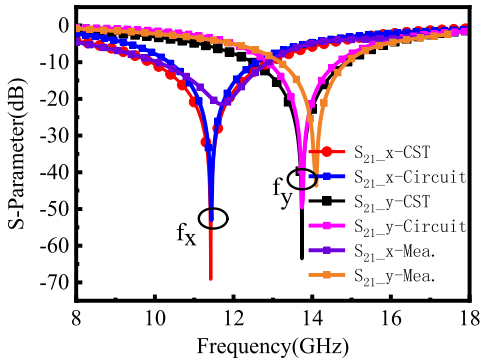

Fig. 2. Transmission characteristic of the bilayer FSS displacement sensor in the initial state. (For x-direction: L=2.96nH, C_g=0.06029pF, C_L=0.009016pF; For y-direction: L=3.94nH, C_g=0.0309pF, C_L=0.0008pF.)

The substrates of the two layers are flexible PDMS with relative permittivity of εr=2.7 and thickness of h=0.2mm.

As shown in Fig.1(b), the FSS based displacement sensor has two layers stacked in z-direction, and the resonators on the top and bottom layer are strip-type multilayer graphene and perpendicular to each other. When electromagnetic waves are incident, only one part of the incident wave is transmitted and another part is reflected, thus the transmission or reflection characteristics of the FSS can be measured wirelessly. And as a displacement sensor, we assume that center alignment of resonators on two layers is the initial state, and the bottom layer is static, while the top layer is dynamic to move. As shown in Fig.1(b), the top layer with red resonators represents that the top layer has moved along x-direction with alignment displacement of Δx, while the layer with green resonators represents there is displacement of Δy along y-direction.

According to the structure of the double-layer FSS based displacement sensor above, the corresponding equivalent circuit can be described as a parallel LC circuit as shown in Fig.1(c), where a rectangular graphene film is equivalent to an inductor L. And the total equivalent capacitance is composed of C_g and C_L, where C_g comes from adjacent resonators in the same direction, while C_L is the capacitance between resonator1 on the top layer and resonator2 on the bottom layer. The resonant frequencies of the bilayer FSS based sensor can be approximately expressed as:

$$f = \frac{1}{2\pi\sqrt{L\left(C_g + C_L\right)}} \tag{1}$$

Due to C_g and the equivalent inductance L are related the physical dimensions of each layer of the FSS, they are not changed with different displacement between two layers. Meanwhile, the C_L changes with the displacement between two layers.

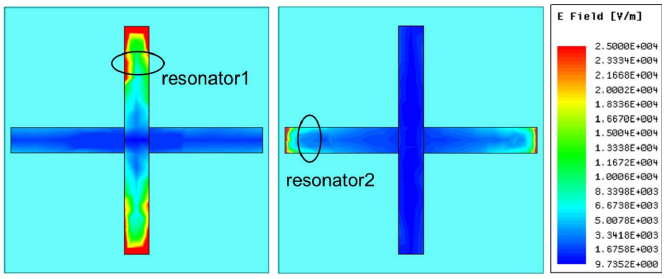

Fig. 3. The electric field distribution at each resonant frequencies.

The design and optimization of the FSS are performed in CST Microwave Studio using periodic boundary conditions in x and y-directions and open in z-direction, and the frequency-domain finite element method (FEM) is used. The corresponding transmission characteristics of the initial state of the FSS based displacement sensor are shown in Fig.2, where S_{21}_x is the transmission parameter of the FSS excited by x-polarization incident wave, and S_{21}_y represents the transmission parameter of the FSS under the excitation of y-polarization incident wave. The two resonant frequencies that f_x=11.4 GHz and f_y=13.8GHz correspond to the resonant frequencies of the bottom layer with resonator 2 and top layer with resonator 1 respectively. The parameter values in the equivalent circuit are extracted by using optimization algorithm to adjust the circuit simulation curves in Microwave Office software to fit the EM simulation curves of CST Microwave Studio. It can be seen that the circuit simulation is consistent with the EM simulation and measurement results, in which the circuit simulation and CST calculation results are almost identical. However, the resonant depth of the measured curve is small, and the resonant frequency is slightly shifted to the high frequency, which may be caused by the error of experiment and manufacture. Another reason is that the periodic boundary condition is applied in the simulation, while the sample in the actual measurement is limited in size.

The electric field distribution characteristics of the FSS at each resonant frequency in shown in Fig.3, we can notice that the x or y-direction displacement between two layers will change the C_L between resonator1 and resonator2, which will bring a shift of the resonant frequency of the FSS based sensor, as described in (1). Due to the polarization-related characteristic of the FSS, the displacement in x/y-direction can only change the resonant frequency of the resonator along x /y-direction. Therefore, the polarization and the resonance characteristics of the double-layer FSS can be applied to wireless displacement sensor design.

III. Simulation Results

A. Displacement in x Direction

In simulation, we keep the bottom layer of FSS static and move the top layer in x or y-direction. The transmission curves of the double-layer FSS with x-direction displacement is shown in Fig. 4. If the FSS based sensor is incident through x-polarization incident wave, there is x-direction displacement Δx varying from 0 to 5.25mm between two layers, the non-resonant resonator1 on top layer moves toward to

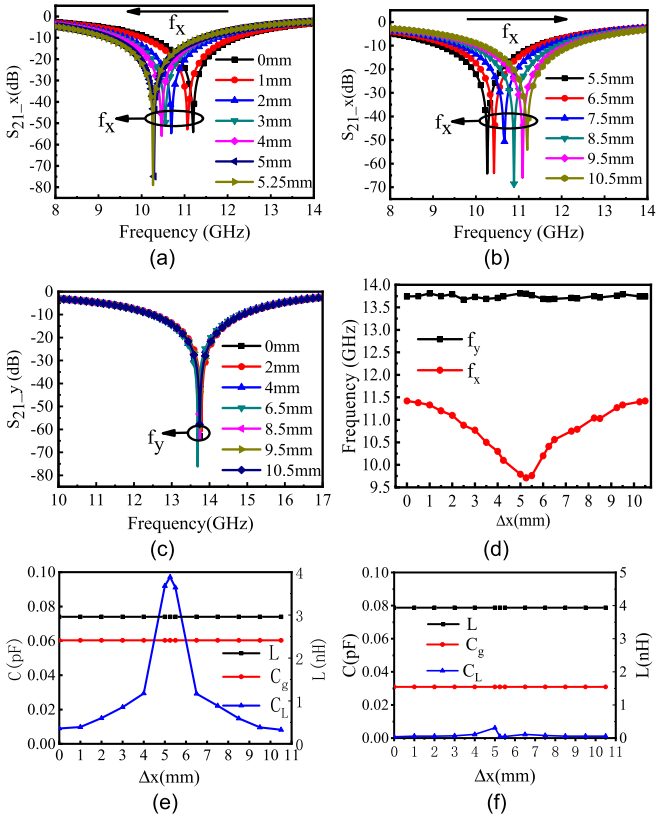

Fig. 4. The FSS based sensor with x-direction displacement between two layers: (a) Variation of S_{21}_x with Δx from 0mm to 5.25mm; (b) Variation of S_{21}_x with Δx from 5.5mm to 10.5mm; (c) Variation of S_{21}_y and (d) f_x and f_y with Δx from 0mm to 10.5mm; (e) Variation of equivalent circuit parameters with Δx in the x, and (f) y-directions.

the ends of resonator 2. The electric potential difference between resonator 1 and resonator 2 becomes larger with the increasing Δx, which also means that the capacitance C_L becomes larger, as shown in Fig.4 (e). So we can observe that within x-displacement from 0mm to 5.25mm the resonant frequency f_x shift from 11.42GHz to lower frequency 9.79 GHz, as shown in Fig. 4(a). However, when Δx is increased to more than half period length of the FSS from 5.5mm to 10.5mm, because of the periodicity characteristic, resonator 1 on top layer starts to move from the end to the center of resonator 2 on bottom layer. Similarly, from Fig. 4(e) we can see that the capacitance C_L becomes smaller within this displacement range. Thus from Fig. 4(b) we can see that f_x shifts to higher frequency with increased displacement.

It is noticeable that in the whole displacement range from 0mm to 10.5mm, the change of Δx has little or no impact on non-resonant resonator 2, and as shown in Fig. 4(c) the resonant frequency f_y keeps almost unchanged. Meanwhile, as shown in Fig. 4(f), the inductance L, capacitance C_L and C_g of resonator 2 are basically unchanged. The variation trend of f_x and f_y with x-direction displacement Δx changing from 0 to 10.5mm is shown in Fig. 4(d).

B. Displacement in y Direction

When there is y-direction displacement Δy between two layers, the simulated transmission curves changing with Δy are shown in Fig. 5. Similarly, if there is y-polarization

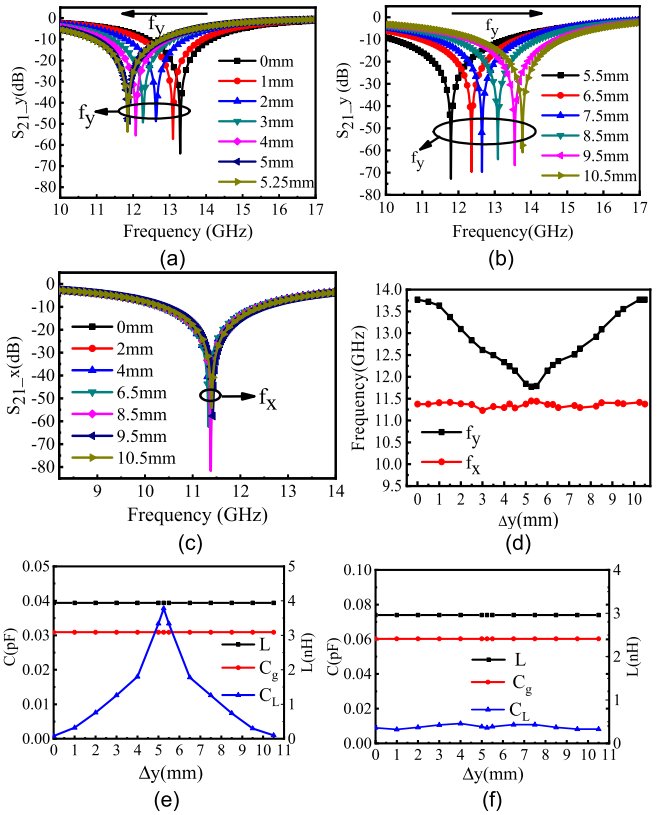

Fig. 5. The FSS based sensor with y-direction displacement between two layers: (a) Variation of S_{21}_y with Δy from 0mm to 5.25mm; (b) Variation of S_{21}_y with Δy from 5.5mm to 10.5mm; (c) Variation of S_{21}_x and (d) f_x and f_y with Δy from 0mm to 10.5mm; (e) Variation of equivalent circuit parameters with Δy in the y, and (f) x-directions.

incident wave, with increased Δy from 0 mm to 5.25mm, resonator 2 on the bottom layer get closer to the end of resonator 1 on the top layer. The capacitance C_L between two resonators becomes larger, thus resonant frequency f_y moves from 13.77GHz to 11.84GHz, as shown in Fig. 5(a) and (e). Because of the periodicity and symmetry of the FSS based displacement sensor, when Δy is increased to more than 5.25mm, C_L between two resonators start to decrease, as shown in Fig.5 (e). Thus f_y moves to higher frequency with Δy increased from 5.5mm to 10.5mm, as presented in Fig. 5(b).

If x-polarization incident wave is used to excite the FSS based sensor, with Δy changes from 0 mm to 10.5mm, the loaded capacitance C_L remains almost constant, and f_y keeps almost unchanged, as shown in Fig. 5(c) and Fig.5 (f). And the variation of resonant frequencies f_x and f_y changes with the y-direction displacement Δy is shown in Fig. 5(d).

As can be seen from Fig. 4 and Fig. 5, the displacement in the x(y)-direction, f_y (f_x), is almost constant. However, it is not difficult to see that f_y (f_x) still has slight fluctuations due to the unnecessary coupling between the upper and lower layers. Therefore, the sensor is not suitable for displacement sensing of orders of magnitude smaller than a few millimeters.

C. Simulated Performance

According to the simulated results, we find that the FSS based sensor can achieve two-dimensional displacement write sensing, and the displacement direction can be easily distinguished from the variation trend of f_x and f_y. Specifically, if there is an obvious shift of f_y while f_x is almost unchanged at same time, it means that there is a displacement in y direction. And the shift trend of f_x and f_y in the x-direction displacement is contrary to the one with displacement in y-direction.

And both the dynamic range with displacement in x or y-direction is 5.25mm, which is limited by the half length of the period of FSS. The sensitivity (S) and the relative sensitivity ($S_{\_res}$) of the FSS based displacement sensor at each direction can be defined as the resonant frequency change per millimeter and the sensitivity at each point divided by the resonance frequency at that point, respectively:

$$S_{x,y} = \frac{\Delta f_{x,y}}{\Delta x,\, y} \tag{2}$$

$$S_{x,y\_res} = \frac{S_{x,y}}{f_{x,y}} \tag{3}$$

where $\Delta f_{x,y}$ represents the resonant frequency shift compared with the initial state in both x and y-directions respectively. It can be expressed as $\Delta f_{x,y} = f_{x,y\_h} - f_{x,y\_l}$, where f_{x,y_h} represents the value corresponding to the high frequency within the frequency response range, and f_{x,y_l} represents the value corresponding to the low frequency within the frequency response range. In (3), $f_{x,y}$ is the resonance frequency in x or y-direction. According to the above formula, it can be calculated from Fig. 4 and Fig. 5 that within the dynamic range of 5mm, the FSS based displacement sensor shows high sensitivity of 326MHz/mm in x-direction and 385MHz/mm in y-direction. And its relative sensitivity in the x and y-directions is 3.07%/mm and 3%/mm, respectively.

IV. Prototype and Experimental Measurement

To verify the performances presented in simulation, the FSS based displacement sensor shown in Fig. 1 is fabricated and measured. Specially, the strip-type resonators on two layers of the sensor are made of multi-layer graphene film, which has high conductivity of about 10^6 S/m. What's more, the graphene film is not only lightweight, but also has high chemical resistance and excellent mechanical stability which is superior to ordinary copper film [32], [33]. The density of ordinary copper film is 8.74g/cm^3, while the density of graphene film is 1.47g/cm^3, which is only one fifth of that of copper film, and has a great lightweight advantage. The experimental results show that the graphene film still has good flexibility after 1000 bends, and its electrical conductivity remains unchanged. Commercial copper film of the same thickness, however, can be bent 28 times before it breaks and is unusable [34]. Moreover, graphene film is also highly resistant to chemical corrosion. According to the experimental study in [35], the graphene film and commercial aluminum film are placed in the same concentration of hydrochloric acid. After 48 hours, the aluminum film is completely corroded, while the graphene film still remains intact. Therefore, the multi-layer graphene film is good substitute of copper film especially in harsh environments.

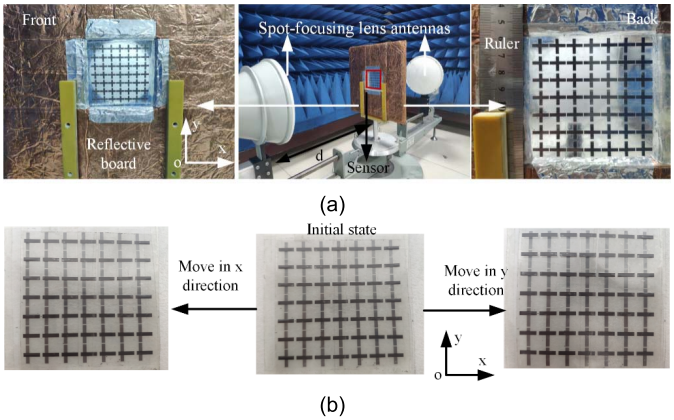

Fig. 6. (a) Experimental setup of the graphene-based FSS wireless displacement sensor; (b) Displacement in x and y-directions between two layers.

The horn antenna is usually used in the electromagnetic characteristic measurement of FSS wireless stress sensor. However, in order to achieve plane wave incidence, the far field condition needs to be satisfied, that is, the distance d between the horn antenna and the test sample needs to meet $d>2A^2/\lambda$, where A is the aperture area of the horn antenna and λ is the wavelength, so the measuring distance required in a specific frequency band is relatively large. By using the focusing lens horn antenna for measuring, as long as the distance between the antenna and the test sample meet the focal length of the lens, an approximate plane wave incident can be formed at the distance from the focal length of the lens, which can reduce the space required for testing. Therefore, a pair of DBT-SFLHA180-400 focusing lens horn antennas working at 8-18GHz are used in this experiment, as shown in Fig. 6(a). Its focal length is 313.5mm, and energy is collected at the position longer from its focal length to form a focal spot with a diameter of 50mm.The size of the FSS sample is 7 × 7 units, and the size is about 75mm×75mm, which can completely cover the focal spots of the horn antennas and make them form plane wave incidence on the FSS. At the same time, the antennas are connected to the two ports of the vector network analyzer (Anritsu MS46322A) respectively to test the electromagnetic characteristics of the FSS.

As shown in Fig. 6(b), in the displacement sensing experiment, firstly resonator1 on the top layer is put perpendicularly with resonator2 on the bottom layer, and set the center alignment of resonator1 and resonator2 as the initial state of the sensor. Regarding the displacement between top and bottom layers, the x or y-direction displacement in a dynamic range of 5mm is realized by keeping the bottom layer static and moving the top layer manually.

When the top layer moves toward x-direction in the dynamic range of 5mm, the variations of transmission parameters with x-polarization and y-polarization incident wave are shown in Fig. 7. Firstly, we find that the measured resonant frequencies f_x and f_y in the initial state of the sensor are 11.75GHz and 14.15GHz, respectively. And in the whole displacement range from 0mm to 5mm, as shown in Fig.7 (a) and (b), respectively, the resonant frequency f_x is moving from 11.75GHz to

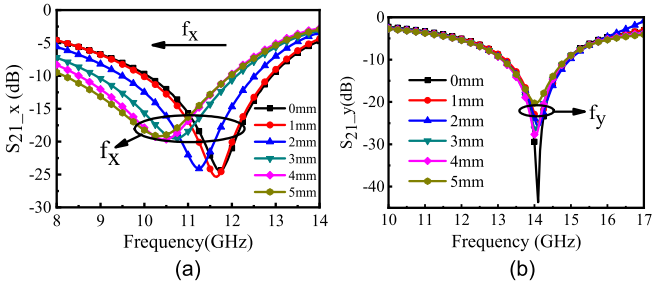

Fig. 7. Measured transmission parameters of the FSS-based sensor with x-direction displacement from 0mm to 5mm: (a) Variation of S_{21}_x; (b) Variation of S_{21}_y.

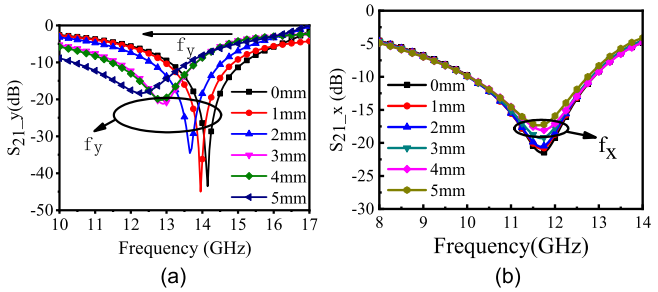

Fig. 8. Measured transmission parameters of the FSS-based sensor with y-direction displacement from 0mm to 5mm: (a) Variation of S_{21}_y; (b) Variation of S_{21}_x.

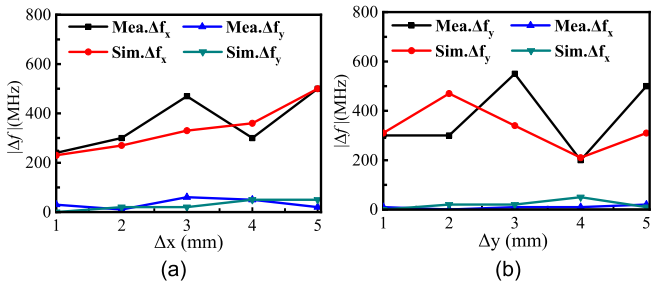

Fig. 9. Measured and simulated frequency changes versus displacement of the sensor based on FSS from 0mm to 5mm: (a) x-direction displacement; (b) y-direction displacement.

10.35GHz gradually, while resonant frequency f_y is stable around 14.15GHz. The measured variation trends of f_x and f_y are in good agreement with the simulated results, and it shows sensitivity of 280MHz/mm and relative sensitivity of 2.42%/mm in x-direction.

When there is displacement in y direction, the measured transmission parameters excited by y-polarization incident waves are shown in Fig.8. With the increase of y-direction displacement from 0mm to 5mm, it can be obviously observed that f_y shifts from 14.15GHz to 12.3GHz gradually, as shown in Fig.8 (a). Meanwhile, from Fig. 8 (b) we can see that f_x is almost unchanged. Therefore, the variation trends of f_x and f_y with y-direction displacement are also consistent with the simulated results. And the measured results with y-direction displacement presents sensitivity of 370MHz/mm and relative sensitivity of 2.8%/mm.

The response curves of frequency changes versus displacement of the FSS based sensor are shown in Fig. 9,

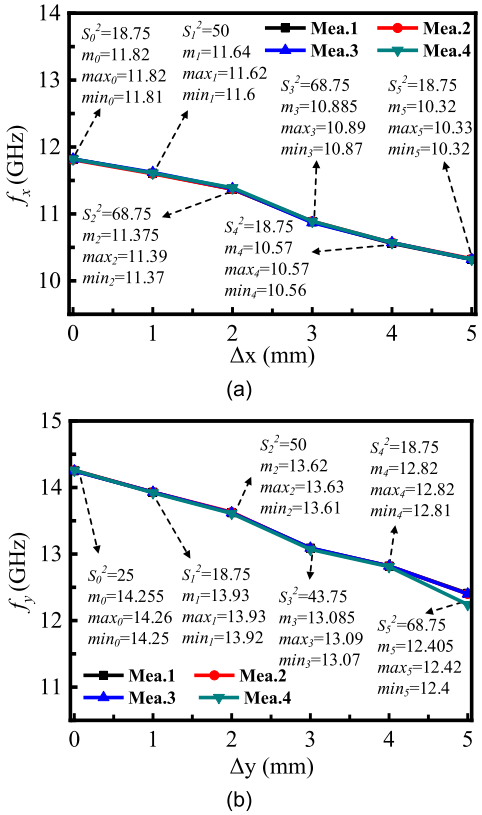

Fig. 10. Frequency curve of the sensor based on FSS with displacement from 0mm to 5mm at four measurements: (a) x-direction displacement; (b) y-direction displacement.

TABLE II
NONLINEARITY ERROR (δ) FOR EACH DISPLACEMENT POINT

	0mm	1mm	2mm	3mm	4mm	5mm
δ_{x_Sim}	6.69%	4.35%	4.09%	2.61%	2.61%	3.48%
δ_{x_Mea}	5.06%	5.06%	3.02%	6.74%	5.6%	2.21%
δ_{y_Sim}	2.18%	5.1%	0.73%	0	5.83%	4.37%
δ_{y_Mea}	1.9%	1.4%	5.71%	6%	4.61%	3.9%

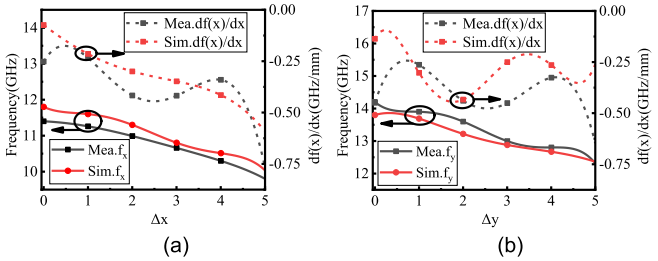

Fig. 11. Measured and simulated frequency variation characteristics and their derivatives with (a) x-direction displacement and (b) y-direction displacement from 0mm to 5mm after curve fitting of the sensor based on FSS.

in which Fig. 9 (a) and (b) show the variation of frequency changes with the displacement in x-direction and y-direction respectively. Here, $|\Delta f_x|$ and $|\Delta f_y|$ represent the frequency changes with the displacement in x-direction and y-direction respectively. As shown in Fig. 9(a), when a displacement of 1mm to 5mm is generated in the x-direction, the maximum difference of $|\Delta f_x|$ obtained from the simulation and measurement results is 250MHz and 260MHz respectively. Similarly, the maximum difference of $|\Delta f_y|$ obtained from simulation and measurement results in the y-direction is 260MHz and 270MHz respectively. It can be seen from Fig. 9 that the change of $|\Delta f|$ is not stable, because the resonant frequency is 11.4GHz and 13.8GHz respectively when the relative displacement is generated in x and y-direction. For this band, a fluctuation of about 0.2GHz is acceptable in our practical application.

Meanwhile, we have measured the sensor for several times under the same measuring environment, and four groups of measurement results are shown in Fig. 10. Mea.1, Mea.2, Mea.3 and Mea.4 in Fig. 10 are the result curves obtained from four measurements respectively. In order to characterize the precision characteristic of the sensor, the variance (s^2), median (m), maximum (max) and minimum (min) values of each set of measured data are calculated. The calculation results are also marked in Fig. 10, where s_i^2 ($i = 0, 1, 2, 3, 4, 5$) is the variance of the point when the displacement is i mm, and its unit is MHz^2. Here m, max and min are all in GHz. The results show that the data of each displacement point of the sensor have good consistency and high repeatability in the actual measurement.

In order to characterize the sensitivity of the sensor more intuitively, the curve of the sensitivity changing with the displacement distance is given, as shown in Fig. 11. This work was carried out in MATLAB, and the curve fitting toolkit in MATLAB was used to fit the response of frequency variation with displacement distance obtained by simulation and measurement into a fifth-order polynomial, making the curves smoother. Since the displacement generated in the x-direction does not affect the change of f_y, we only fit the curve of the variation of f_x in the x-direction here, and similarly, we only fit the curve of the variation of f_y in the y-direction. Fig. 11 (a) and (b) are polynomial fitting results of frequency variation curve with displacement in x and y-directions respectively, and their derivatives are obtained respectively. According to the results in Fig. 11, the measured and simulated nonlinear errors (δ) of each displacement point in x and y-directions can be calculated by (4):

$$\delta_{x,y\_Sim/Mea} = \frac{\left| f_{x,y\_Sim/Mea} - f_{IL} \right|}{F_{x,y\_Sim/Mea}} \tag{4}$$

which is shown in Table II. Among them, f_{x_Sim} and f_{x_Mea} are the resonant frequencies obtained by simulation and measurement at a certain displacement point in the x-direction respectively, f_{IL} represents the frequency when the curve is ideal linear, and F_x is the maximum resonant frequency that can be obtained when the displacement is in the x-direction. Since the change of f_y and f_x caused by displacement in the x and y-directions is almost negligible, and we only

TABLE III
COMPARISON OF THE PERFORMANCE OF THE REPORTED MICROWAVE SENSORS WITH THE PROPOSED ONE

Reference	Sensor type	f_{01} (GHz)	Dimensions	Dynamic range	Sensitivity (/mm)	Wireless	Relative sensitivity(/mm)
[2]	CPW+SRRs	1.17	1D	1.1mm	25dB	No	-
[4]	CPW+SRRs	1.4	1D	5mm	60MHz	No	4.3%
[5]	CPW+EBG	13	1D	2.5mm	40dB	No	-
[9]	ML2+SRRs	2.5	2D	3mm	x: 89MHz y: 70MHz	No	x: 3.56% y: 2.8%
[10]	Dielectric resonator (DR)	3.69	1D	6mm	95MHz	Yes	2.6%
[11]	DR	3.41	1D	7mm	22.9MHz	Yes	0.67%
[15]	Antenna	2.4	1D	7.7mm	0.65MHz	No	0.27%
[28]	Metamaterial	0.4	1D	7mm	8MHz	Yes	2%
This work	Graphene FSS	11/14	2D	5 mm	x: 326MHz y: 385MHz	Yes	x: 3.07% y: 3%

care about the frequency shift caused by displacement in the respective directions, only the nonlinear errors based on f_x and f_y in the x and y-directions are given here respectively. It is obvious from the calculation results of nonlinear errors in Table II that the nonlinear errors in both simulation and measurement in x and y-directions are less than 7%. The maximum nonlinear errors in each direction are derived from the measured results, which are 6.74% in the x-direction and 6% in the y-direction, respectively. Therefore, the sensor not only has high sensitivity, but also has guaranteed accuracy in implementation.

The curve after derivation is the sensitivity curves versus displacement, as shown by the dotted line in Fig. 11. Based to the curves, we can calculate that the average measured and simulated sensitivities of the sensor in the x-direction are 404.85MHz/mm and 323.75MHz/mm respectively, and the average measured and simulated sensitivities in the y-direction are 429.37MHz/mm and 361.72MHz/mm respectively. Obviously, the measured average sensitivity here is higher than that of the simulation. It can be seen from the curves variation that this is caused by the large fluctuation of frequency variation in the measured data, which may be due to the error caused by manually adjusting the relative distance between the upper and lower FSS in the measurement.

Compared with the simulated results, the measured counterparts are about 300MHz higher than the simulated ones on average within the displacement range of 0-5mm, especially the deviation at high frequencies is large. One is due to the experimental and manufacturing errors, mainly from the slight deviation when manually adjusting the relative displacement distances of upper and lower FSS. Another is due to that the corresponding frequency is high when it produces small displacement changes, hence the relative error is also increased. Furthermore, it is obvious that the resonance depth of the FSS measured is not as good as that of the simulation, due to the influence of the measured environment and the difference between the 7×7 array in the measurement and the infinite period array in the simulation. From the measured results, we find that although there are some frequency shift errors, we can always distinguish the direction of the displacement from the variation trend of f_x and f_y. and in the dynamic range of 5mm, both the sensitivities with x and y-directions displacement are very high. What's more, it is worthy noticing that in experiment, there is no extra cables connected to the sensor, namely it can be wirelessly measured, making the installation and measurement easier.

V. CONCLUSION

In this paper, a wireless two-dimensional displacement sensor using bilayer graphene-based FSS with high sensitivity is designed, simulated and experimentally demonstrated. The performance comparison between the reported microwave displacement sensors and the proposed displacement sensor is shown in Table III, it is obvious that the proposed graphene FSS based displacement sensor has following advantages: Firstly, it can achieve two-dimensional displacement sensing, and the direction of displacement can be distinguished by the variation trend of resonant frequencies. Secondly, in the dynamic range of 5mm it shows high sensitivity of 326MHz/mm in x-direction and 385MHz/mm in y-direction. Thirdly, the displacement sensing can be measured wirelessly, which bring much convenience for practical applications. Finally, due to the good chemical and mechanical performance of the multi-layer graphene film, it has potential of working in harsh environments, showing great application prospects.

REFERENCES

[1] J. Naqui, M. Durán-Sindreu, and F. Martín, "Alignment and position sensors based on split ring resonators," *Sensors*, vol. 12, no. 9, pp. 11790–11797, Aug. 2012.

[2] A. K. Horestani, C. Fumeaux, S. F. Al-Sarawi, and D. Abbott, "Displacement sensor based on diamond-shaped tapered split ring resonator," *IEEE Sensors J.*, vol. 13, no. 4, pp. 1153–1160, Apr. 2013.

[3] S. Harnsoongnoen and N. Angkawisittpan, "Angular displacement sensor based on coplanar waveguide (CPWs) loaded with S-shaped golden spiral-tapered split ring resonators (SGS-SRRs)," *Proc. Comput. Sci.*, vol. 86, pp. 75–78, Jan. 2016.

[4] A. K. Horestani, Z. Shaterian, and F. Martin, "Detection modalities of displacement sensors based on split ring resonators: Pros and cons," in *Proc. Int. Conf. Electromagn. Adv. Appl. (ICEAA)*, Sep. 2019, pp. 479–484.

[5] M. Joodaki and M. Rezaee, "Coplanar waveguide (CPW) loaded with an electromagnetic bandgap (EBG) structure: Modeling and application to displacement sensor," *IEEE Sensors J.*, vol. 16, no. 9, pp. 3034–3040, May 2016.

[6] J. Basseri and M. Joodaki, "An angular displacement sensor with a curved two-metal-layer CPW loaded by an EBG structure," *IEEE Sensors J.*, vol. 18, no. 6, pp. 2335–2341, Jan. 2018.

[7] M. Rezaee and M. Joodaki, "Two-dimensional displacement sensor based on CPW line loaded by defected ground structure with two separated transmission zeroes," *IEEE Sensors J.*, vol. 17, no. 4, pp. 994–999, Feb. 2017.

[8] J. Naqui and F. Martín, "Angular displacement and velocity sensors based on electric-LC (ELC) loaded microstrip lines," *IEEE Sensors J.*, vol. 14, no. 4, pp. 939–940, Apr. 2014.

[9] A. K. Horestani, J. Naqui, Z. Shaterian, D. Abbott, C. Fumeaux, and F. Martín, "Two-dimensional alignment and displacement sensor based on movable broadside-coupled split ring resonators," *Sens. Actuators A, Phys.*, vol. 210, pp. 18–24, Apr. 2014.

[10] A. V. Praveen Kumar and P. Regalla, "A transmission mode dielectric resonator as a displacement sensor," *IEEE Sensors J.*, vol. 20, no. 13, pp. 6979–6984, Jul. 2020.

[11] A. V. Praveen Kumar and A. K. Ojha, "A microstrip coupled cylindrical dielectric resonator as a displacement sensor," *IETE J. Res.*, vol. 4, pp. 1–7, Mar. 2019.

[12] H.-X. Zhu, P. Cheong, K.-W. Tam, S.-K. Ho, and W.-W. Choi, "An angular displacement sensor based on microstrip wideband impedance transformer with quasi-chebyshev frequency response," *IEEE Sensors J.*, vol. 20, no. 8, pp. 4200–4206, Apr. 2020.

[13] S. F. Wang *et al.*, "Theoretical analyses and experimental evaluation of a small-displacement sensor based on surface plasmon resonance technology," *Sens. Mater.*, vol. 26, pp. 371–377, Oct. 2014.

[14] E. Asua, V. Etxebarria, A. García-Arribas, J. Feutchwanger, J. Portilla, and J. Lucas, "Interface electronics for an RF resonance-based displacement sensor," *J. Phys., Conf. Ser.*, vol. 450, Jun. 2013, Art. no. 012017.

[15] Xue, Yi, Xie, Wan, and Ding, "A displacement sensor based on a normal mode helical antenna," *Sensors*, vol. 19, no. 17, p. 3767, Aug. 2019.

[16] S. Guan, L. Xie, S. Xue, and G. Wan, "Displacement sensor based on separated inverted-F antenna," in *Proc. IEEE Int. Conf. Comput. Electromagn. (ICCEM)*, Mar. 2019, pp. 1–3.

[17] J. A. Rice *et al.*, "A wireless multifunctional radar-based displacement sensor for structural health monitoring," *Proc. SPIE Sensors Smart Struct. Technol. Civil, Mech., Aerosp. Syst.*, vol. 7981, Apr. 2011, Art. no. 79810K.

[18] N. Blar *et al.*, "Modeling and characterization of LC displacement sensor in PCB technology," in *Proc. 35th Int. Spring Seminar Electron. Technol.*, Oct. 2012, pp. 394–398.

[19] R. Bhattacharyya, C. Floerkemeier, and S. Sarma, "Towards tag antenna based sensing—An RFID displacement sensor," in *Proc. IEEE Int. Conf. RFID*, Apr. 2009, pp. 95–102.

[20] N. Liu, X. Sheng, C. Zhang, and D. Guo, "Design of frequency selective surface structure with high angular stability for radome application," *IEEE Antennas Wireless Propag. Lett.*, vol. 17, no. 1, pp. 138–141, Jan. 2018.

[21] K. Zhang, W. Jiang, and S. Gong, "Design bandpass frequency selective surface absorber using LC resonators," *IEEE Antennas Wireless Propag. Lett.*, vol. 16, pp. 2586–2589, 2017.

[22] B. Wu, Y.-J. Yang, H.-L. Li, Y.-T. Zhao, C. Fan, and W.-B. Lu, "Low-loss dual-polarized frequency-selective rasorber with graphene-based planar resistor," *IEEE Trans. Antennas Propag.*, vol. 68, no. 11, pp. 7439–7446, Nov. 2020.

[23] C. Yang, X.-W. Zhu, P. Liu, W. Hong, H. Feng, and Y. Shi, "A circularly polarized horn antenna based on an FSS polarization converter," *IEEE Antennas Wireless Propag. Lett.*, vol. 19, no. 2, pp. 277–281, Feb. 2020.

[24] I. A. I. Al-Naib, C. Jansen, and M. Koch, "Thin-film sensing with planar asymmetric metamaterial resonators," *Appl. Phys. Lett.*, vol. 93, no. 8, Aug. 2008, Art. no. 083507.

[25] P. Rodriguez-Ulibarri, A. Urrutia, S. A. Kuznetsov, and M. Beruete, "THz thin film sensing with labyrinth metasurface absorber," in *Proc. 13th Eur. Conf. Antennas Propag.*, 2019, pp. 1–3.

[26] C. Debus and P. H. Bolivar, "Frequency selective surfaces for high sensitivity terahertz sensing," *Appl. Phys. Lett.*, vol. 91, no. 18, Oct. 2007, Art. no. 184102.

[27] R. Melik *et al.*, "Metamaterial based telemetric strain sensing in different materials," *Opt. Exp.*, vol. 18, no. 5, pp. 5000–5007, 2010.

[28] B. Ozbey *et al.*, "Wireless displacement sensing enabled by metamaterial probes for remote structural health monitoring," *Sensors*, vol. 14, no. 1, pp. 1691–1704, 2014.

[29] D. Hasan and C. Lee, "Hybrid metamaterial absorber platform for sensing of CO_2 gas at mid-IR," *Adv. Sci.*, vol. 5, no. 5, May 2018, Art. no. 1700581.

[30] W. He *et al.*, "Sensors with multifold nanorod metasurfaces array based on hyperbolic metamaterials," *IEEE Sensors J.*, vol. 20, no. 4, pp. 1801–1806, Feb. 2020.

[31] C. R. Farrar and K. Worden, "An introduction to structural health monitoring," *Philos. Trans. Roy. Soc. London A, Math. Phys. Sci.*, vol. 365, no. 1851, pp. 303–315, 2007.

[32] S. Asgari and T. Fabritius, "Equivalent circuit model of graphene chiral multi-band metadevice absorber composed of U-shaped resonator array," *Opt. Exp.*, vol. 28, no. 26, p. 39850, Dec. 2020.

[33] S. Asgari and T. Fabritius, "Tunable mid-infrared graphene plasmonic cross-shaped resonator for demultiplexing application," *Appl. Sci.*, vol. 10, no. 3, p. 1193, Feb. 2020.

[34] H.-R. Zu, B. Wu, Y.-H. Zhang, Y.-T. Zhao, R.-G. Song, and D.-P. He, "Circularly polarized wearable antenna with low profile and low specific absorption rate using highly conductive graphene film," *IEEE Antennas Wireless Propag. Lett.*, vol. 19, no. 12, pp. 2354–2358, Dec. 2020.

[35] R. Song *et al.*, "Sandwiched graphene clad laminate: A binder-free flexible printed circuit board for 5G antenna application," *Adv. Eng. Mater.*, vol. 22, no. 10, Oct. 2020, Art. no. 2000451.

Jun-Jie Zhang was born in Dazhou, Sichuan, China, in 1997. She received the B.S. degree in electronic engineering from the University of South China, Hengyang, China, in 2019. She is currently pursuing the M.S. degree in electromagnetic fields and microwave technology with Xidian University. Her research interests include graphene-based microwave devices and polarization converting metasurface and reflectarray.

Bian Wu (Senior Member, IEEE) was born in Xianning, Hubei, China, in 1981. He received the B.S. and Ph.D. degrees in electromagnetic fields and microwave technology from Xidian University, Xi'an, China, in 2004 and 2008, respectively. Since 2008, he has been worked with Xidian University. From March 2013 to February 2014, he was a Postdoctoral Visitor with Queen Mary University of London, U.K. He is currently a Professor and a Ph.D. Supervisor with the National Key Laboratory of Antennas and Microwave Technology, Xidian University. He has authored or coauthored over 100 journal publications. His research interests include microwave circuits and devices, filtering antennas, metamaterials, and graphene-based devices.

Yu-Tong Zhao received the B.E. degree in electronic engineering and the Ph.D. degree in electromagnetic fields and microwave technology from Xidian University, Xi'an, China, in 2013 and 2018, respectively. He is currently focused on graphene-based devices, millimeter-wave and terahertz imaging, metamaterials, and RF design.

Lei Song was born in Xi'an, Shaanxi, China, in 1995. She received the B.S. degree in electronic engineering and the M.S. degree in electromagnetic fields and microwave technology from Xidian University, Xi'an, China, in 2017 and 2020, respectively. Her research interests include frequency selective surfaces, graphene-based microwave, and THz devices.

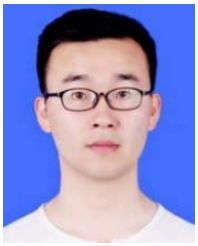

Rong-Guo Song received the Master of Science degree from the School of Science, Wuhan University of Technology, Wuhan, China, in 2018. He is currently pursuing the Ph.D. degree with Hubei Engineering Research Center of RF-Microwave Technology and Application, Wuhan University of Technology. His research interests include graphene based materials and RF and microwave devices design.

Hao-Ran Zu was born in Jiangsu, China, in 1994. He received the B.S. degree in electromagnetic fields and radio technology from Chongqing University of Posts and Telecommunications, Chongqing, China, in 2017. He is currently pursuing the Ph.D. degree in electromagnetic fields and microwave technology with the National Key Laboratory of Antennas and Microwave Technology, Xidian University. His research interests include antenna design and microwave devices based on spoof surface plasmon polaritons.

Da-Ping He received the Ph.D. degree in materials processing engineering from WUT in 2013. He was a Postdoctoral Fellow with the University of Science and Technology of China. Then, he joined the University of Bath as a Newton International Fellow and the University of Cambridge as a Postdoctoral Fellow. He is a Full Professor at WUT. His research interests are preparation and application of nano-composite materials into new energy devices, sensors, and RF microwaves field.